SCIENTIFIC REPORTS

Correction: Author Correction

OPEN

Spin-orbit-torque-induced magnetic domain wall motion in Ta/CoFe nanowires with sloped perpendicular magnetic anisotropy

Yue Zhang[1,2], Shijiang Luo[1], Xiaofei Yang[1] & Chang Yang[3]

In materials with the gradient of magnetic anisotropy, spin-orbit-torque-induced magnetization behaviour has attracted attention because of its intriguing scientific principle and potential application. Most of the magnetization behaviours microscopically originate from magnetic domain wall motion, which can be precisely depicted using the standard cooperative coordinate method (CCM). However, the domain wall motion in materials with the gradient of magnetic anisotropy using the CCM remains lack of investigation. In this paper, by adopting CCM, we established a set of equations to quantitatively depict the spin-orbit-torque-induced motion of domain walls in a Ta/CoFe nanotrack with weak Dzyaloshinskii–Moriya interaction and magnetic anisotropy gradient. The equations were solved numerically, and the solutions are similar to those of a micromagnetic simulation. The results indicate that the enhanced anisotropy along the track acts as a barrier to inhibit the motion of the domain wall. In contrast, the domain wall can be pushed to move in a direction with reduced anisotropy, with the velocity being accelerated by more than twice compared with that for the constant anisotropy case. This substantial velocity manipulation by anisotropy engineering is important in designing novel magnetic information devices with high reading speeds.

Since the concept of "race-track storage" was proposed in 2008[1], current-induced magnetic domain wall motion in nanotracks has attracted wide research interest because of its application potential in next-generation memory-storage devices with advantages such as low dissipation, high reading speed, small size, and large storage density. The basic physical principle underlying such devices is the exchange of angular momentum between the spins of conducting electrons and magnetic moments in the domain wall due to the spin-transfer torque (STT) or spin-orbit torque (SOT). Recently, SOT-driven domain wall motion has attracted wide attention because of its high energy efficiency[2–4].

Unlike the bulk STT in a single ferromagnetic nanotrack, the SOT dominates in multilayer films, such as heavy metal (HM)/ferromagnet (FM) multilayer[2, 3, 5] or HM/FM/oxide multilayer with broken inversion symmetry at the interface[4]. The SOT effect in the multilayer system can originate from the spin Hall effect (SHE) of the HM layer. Recently, some intriguing SOT-induced magnetization behaviours have been discovered in HM/FM bi-layers with *sloped* magnetic parameters. For example, Yu *et al.* discovered field-free magnetization switching in a Ta/CoFeB perpendicularly magnetized (PM) film with magnetic anisotropy gradient[6]. They attributed this phenomenon to an effective magnetic field originating from the gradient of the magnetic anisotropy constant.

From a microscopic perspective, the SOT-induced magnetizing process in a HM/FM multilayer is generally related to the motion of the FM domain wall. For example, the domain wall exhibits chirality and an unexpected Néel-typed structure in the HM/FM multilayer with interfacial Dzyaloshinskii–Moriya interaction (DMI)[3, 7]. The direction of the motion of the domain wall is also related to the sign of the DMI constant and to that of the spin Hall angle of the HM[4, 8–10]. In addition, the domain wall also tilts because of strong DMI, which has been experimentally observed[11, 12] and theoretically proven[9, 13–16]. Additionally, domain wall motion is closely linked to the

[1]School of Optical and Electronic Information, Huazhong University of Science and Technology, Wuhan, 430074, PR China. [2]Department of Physics and Astronomy, Johns Hopkins University, Baltimore, MD, 21218, USA. [3]Department of Mathematics, Harbin Institute of Technology, Harbin, 150001, PR China. Correspondence and requests for materials should be addressed to C.Y. (email: yangchang@hit.edu.cn)
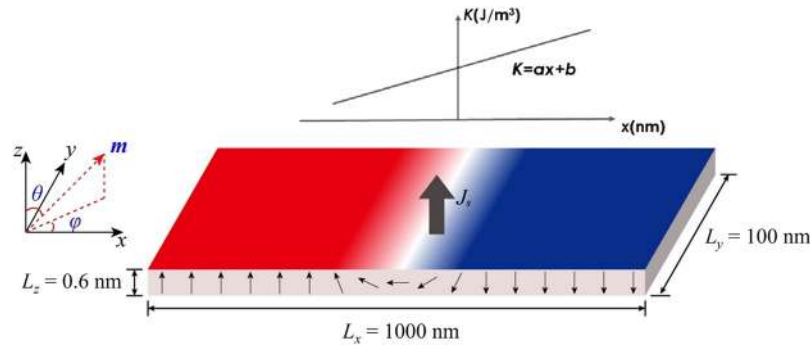
Figure 1. Schematic of SOT-driven domain wall in a nanotrack with magnetic anisotropy gradient. (The theoretic analysis in the paper is based on the up-down domain wall structure in the coordinate system shown in Fig. 1).

magnetic anisotropy constant which can be controlled effectively by manipulating the thickness of the film or by being situated in an electric field[17–20].

Despite recent progress, determining how the domain wall moves in a HM/FM multilayer with the gradient of magnetic anisotropy remains to be elucidated. Yamada *et al.* proposed an effective field induced by the gradient of magnetic anisotropy and believe that this effective field can drive the wall to move[21]. However, the domain-wall motion in a magnetic system with anisotropy gradient has not been investigated using standard cooperative coordinate method (CCM), which is the basic route to quantitatively study the domain wall motion[7, 22].

In the present work, using CCM, we have deduced the equations to describe the SOT-driven domain wall motion in a HM/FM multilayer with the gradient of magnetic anisotropy and weak DMI. The equations were solved numerically and compared with the results of a micro-magnetic simulation. Based on the derived equations, the effect of magnetic anisotropy gradient on the domain wall motion has been revealed.

Principle and Methods

Numerical Calculation based on collective coordinate model.

To quantitatively describe the dynamics of SOT-driven domain wall motion in a nanotrack with magnetic anisotropy gradient, we develop a one-dimensional (1D) CCM, where the DW is depicted by two collective coordinates: its central position q and the azimuthal angle φ of the DW magnetization in spherical coordinates, as shown in Fig. 1. Due to the weak DMI, the tilting angle of DW is not taken into consideration here[9].

The normalized vector for the direction of magnetization is described as $\vec{m} = (\sin\theta\cos\varphi, \ \sin\theta\sin\varphi, \ \cos\theta)$. The polar angle θ and the azimuthal angle φ marked in Fig. 1 are included in the ansatz for the DW magnetization:

$$\theta = 2\arctan\{\exp[(x-q)/\Delta]\}, \text{ and } \varphi = \varphi(t) \tag{1}$$

where t is the time, and

$$\Delta = \sqrt{A/(K - \mu_0 M_S^2/2)}, \tag{2}$$

represents the width of the domain wall and A, μ_0, M_S, and K are the exchange stiffness constant, vacuum permeability, saturation magnetization, and magnetic anisotropy constant for the PMA film, respectively. In the present work, $K = ax + b$. This linear function $K(x)$ is the simplest form for numerical calculation. From the aspect of experiments, to generate PM film with linearly varied K, one can fabricate PM film with a gradient of thickness along the track[6] or by poling piezoelectric substrate in a wedge shape[21]. To determine the parameters a and b in the function $K(x)$, one can pattern the sample into an array of Hall bar and fit the K-x relationship composed by the K data collected at different sites (x) using extraordinary Hall effect measurement[6].

The variation of magnetic anisotropy in the track may lead to a space-coordinate dependent φ. However, the width of the domain wall is comparatively smaller than the length of the entire track, and the magnetic anisotropy can remain to be considered constant in the region of the domain wall. Therefore, φ is also approximately invariant in the range of the domain wall.

The Thiele equation for the domain wall motion is deduced by the Lagrangian approach. Let l be the Lagrangian density function and the expression can be written as follows[13]

$$l = E + (M_S/\gamma)\varphi\dot{\theta}\sin\theta, \tag{3}$$

where γ is the gyromagnetic ratio, $\dot{\theta}$ is the time derivative of θ, and E represents the total free energy density and can be written as

$$E = E_e + E_a + E_d + E_{DM}. \tag{4}$$

E_e, E_a, E_d, and E_{DM} are the exchange energy density, magnetic anisotropy energy density, demagnetization energy density, and free energy density from DMI, respectively. They are written as

$$E_e = A \sum_{i=x,y,z} |\nabla m_i|^2, \tag{5}$$

where ∇ is the Nabla symbol.

$$E_a = \left(K - \frac{1}{2}\mu_0 M_S^2\right)\sin^2\theta, \tag{6}$$

$$E_d = \frac{1}{2}\mu_0 N_x M_S^2 \sin^2\theta \, \cos^2\varphi, \tag{7}$$

$$E_{DM} = D[m_z(\partial m_x/\partial x) - m_x(\partial m_z/\partial z)], \tag{8}$$

and the demagnetization factor N_x is described by refs 9, 23

$$N_x = L_z \ln 2/\pi\Delta, \tag{9}$$

where L_z is the thickness of Co layer.

For a non-conservative system, another dissipation density function f_d should be included to depict the dissipation[13]:

$$f_d = (\alpha M_S/2\gamma)[d\vec{m}/dt - (\gamma_0/\alpha)H_{SO}(\vec{m} \times \vec{e}_y)]^2, \tag{10}$$

where α is the damping coefficient, and H_{SO} is the effective magnetic field due to SOT and is written as

$$H_{SO} = \mu_B\theta_{SH}J/\gamma_0 e M_S L_z, \tag{11}$$

where μ_B, θ_{SH}, J, and e are the Bohr magneton, spin Hall angle of the HM layer, current density, and charge of an electron, respectively. The parameter γ_0 is related to γ by $\gamma_0 = \mu_0|\gamma|$.

The Lagrangian (L) and Rayleigh dissipation function (F) were determined by integrating l and f_d with respect to the entire space region for the track. The Thiele equations are finally deduced using the Lagrange–Rayleigh equation:

$$\frac{\partial L}{\partial q_i} - \frac{d}{dt}\left(\frac{\partial L}{\partial \dot{q}_i}\right) + \frac{\partial F}{\partial \dot{q}_i} = 0, \tag{12}$$

where q_i represents the collective coordinate q or φ and t is time.

The domain wall motion in the track with magnetic anisotropy gradient is depicted by the following Thiele equations:

$$
\begin{aligned}
(\alpha M_S I_5/\gamma)\dot{q} + (M_S I_8/\gamma\sqrt{A})\dot{\varphi} = &-A(\partial I_1/\partial q) - a(\partial I_2/\partial q) \\
&- \left(b - \frac{1}{2}\mu_0 M_S^2\right)(\partial I_3/\partial q) \\
&- D\cos\varphi(\partial I_4/\partial q) \\
&- (\mu_0 L_z M_S^2 \cos^2\varphi \ln 2/2\pi\sqrt{A}) \\
&\times (\partial I_8/\partial q) \\
&- (M_S\gamma_0/\gamma)H_{SO}I_7\cos\varphi,
\end{aligned}
\tag{13}
$$

$$
\begin{aligned}
(-M_S I_8/\gamma\sqrt{A})\dot{q} + (\alpha M_S I_3/\gamma)\dot{\varphi} = &D I_4 \sin\varphi + (\mu_0 L_z M_S^2(\ln 2) \\
&\times \cos\varphi\sin\varphi/\pi\sqrt{A})I_8 \\
&+ (M_S\gamma_0/\gamma)H_{SO}I_6\sin\varphi,
\end{aligned}
\tag{14}
$$

where I_1–I_8 are the integrals with the following formulas:

$$
\begin{aligned}
I_1 &= \int_{-\frac{Lx}{2}}^{\frac{Lx}{2}} (\sin^2\theta)\left(\frac{\partial f}{\partial x}\right)^2 dx; \quad I_2 = \int_{-\frac{Lx}{2}}^{\frac{Lx}{2}} x(\sin^2\theta)dx; \quad I_3 = \int_{-\frac{Lx}{2}}^{\frac{Lx}{2}} \sin^2\theta \, dx; \\
I_4 &= \int_{-\frac{Lx}{2}}^{\frac{Lx}{2}} \left(\frac{\partial f}{\partial x}\right)\sin\theta \, dx; \quad I_5 \int_{-\frac{Lx}{2}}^{\frac{Lx}{2}} (\sin^2\theta)\left(\frac{\partial f}{\partial q}\right)^2 dx; \quad I_6 = \int_{-\frac{Lx}{2}}^{\frac{Lx}{2}} \sin\theta\cos\theta \, dx; \\
I_7 &= \int_{-\frac{Lx}{2}}^{\frac{Lx}{2}} \left(\frac{\partial f}{\partial q}\right)\sin\theta \, dx; \quad I_8 = \int_{-\frac{Lx}{2}}^{\frac{Lx}{2}} \sqrt{ax + b - \frac{1}{2}\mu_0 M_S^2}(\sin^2\theta)dx.
\end{aligned}
\tag{15}
$$

Here, L_x is the length of nanotrack, and

$$f = (x - q)\sqrt{ax + b - \frac{1}{2}\mu_0 M_S^2}/\sqrt{A};$$

$$\sin\theta = \frac{2\exp(f)}{1 + [\exp(f)]^2};$$

$$\cos\theta = \frac{1 - [\exp(f)]^2}{1 + [\exp(f)]^2}.$$

(16)

Equations (14) and (15) were solved using a 4th-order Runge–Kutta algorithm with a time step of 1 ps. The integrals I_1–I_8 were numerically evaluated using an adaptive Gauss–Kronrod quadrature. In the calculation, the nanotrack has the dimensions 1 μm (length) × 100 nm (width) × 0.6 nm (thickness). Typical magnetic parameters for PM Ta/CoFe bilayers were used[9]:M_S, b, A, D, and α for CoFe are 7×10^5 A/m, 4.8×10^5 J/m^3, 1×10^{-11} J/m, -0.05 mJ/m^2, and 0.03, respectively. The spin-Hall angle (θ_{SH}) for Ta is -0.11. The slopes for the anisotropy constant (a) are 0, 1×10^{11}, 2×10^{11}, and 3×10^{11} J/m^4. A larger a cannot ensure effective perpendicular magnetic anisotropy throughout the entire track.

Micro-magnetic simulation.   The motion of the domain wall in the nanotrack with magnetic anisotropy gradient was also investigated by micro-magnetic simulation using the software "object-oriented micromagnetic framework" (OOMMF) with code including DMI[24]. The principle of the simulation is based on solving the Gilbert equation

$$\frac{\partial \vec{m}}{\partial t} = -\gamma_0 \vec{m} \times \vec{H}_{\text{eff}} + \alpha(\vec{m} \times \frac{\partial \vec{m}}{\partial t}) + \gamma_0 H_{\text{SO}}(\vec{m} \times (\vec{\sigma} \times \vec{m})),$$

(17)

where $\vec{H}_{\text{eff}}$ is the effective magnetic field derived from the free energy density:

$$\vec{H}_{\text{eff}} = -\frac{1}{\mu_0 M_S}(\frac{\delta E}{\delta \vec{m}}),$$

(18)

which includes the effective field from exchange, magnetic anisotropy, demagnetization, and DMI.

We consider a Ta/CoFe nanotrack whose shape and magnetic parameters are identical to that in numerical calculation. In current OOMMF software, it is not possible to generate magnetic anisotropy constants that change with x continuously. As an approximation to the case of $a = 3 \times 10^{11}$ J/m^4 and $J = \pm 5 \times 10^{11}$ A/m^2 in numerical calculation, we fabricated an anisotropy constant that is a piecewise constant function of x. This piecewise constant function of K can be expressed as follows,

$$K = \begin{cases} 1 \times 10^7 \text{ J/m}^3, & (-500 \text{ nm}, -450 \text{ nm}) \\ K_0, & (-450 \text{ nm}, (-450 + \Delta x) \text{ nm}) \\ K_0 + \Delta K, & ((-450 + \Delta x) \text{ nm}, (-450 + 2\Delta x) \text{ nm}) \\ K_0 + 2\Delta K, & ((-450 + 2\Delta x) \text{ nm}, (-450 + 3\Delta x) \text{ nm}) \\ \cdots\cdots\cdots \\ K_0 + N\Delta K, & ((-450 + N\Delta x) \text{ nm}, (-450 + (N + 1)\Delta x) \text{ nm}) \\ 1 \times 10^7 \text{ J/m}^3, & (450 \text{ nm}, 500 \text{ nm}). \end{cases}$$

(19)

The anisotropy constant close to the two ending points of the track (from -500 to -450 nm and from 450 to 500 nm) was set as large as 1×10^7 J/m^3 to pin boundary moments. The remaining nanotrack ($x = -450$ nm to $x = 450$ nm) was evenly divided into $N + 1$ steps with the size of Δx for every step. The anisotropy constant varies from 3.45×10^5 to 6.0×10^5 J/m^3 in accordance with an even step of ΔK. In our simulation, N includes 35, 17, and 9. Accordingly, Δx includes 25 nm, 50 nm, and 100 nm, and ΔK includes 0.075 J/m^3, 0.15 J/m^3, and 0.3 J/m^3, respectively.

Results

Figure 2 shows the current-induced evolution of the central position of the domain wall in the nanotrack with magnetic anisotropy gradient. The negative (positive) current induces the motion of the domain wall towards the positive (negative) x direction, and this indicates that the domain wall moves along the direction of the moving election but against that of the current. This direction is consistent with that for negative D and negative θ_{SH}[4, 9].

When $a = 0$ J/m^4, a linear t–q relationship is well satisfied except at the initial moving stage ($t < 1$ ns). It is also found that the t-q curves with negative J are symmetric to those with positive J. In other words, the domain wall moves towards opposite directions at the same speed with J of different signs. This result is consistent with the reported ones[3, 11, 13] and is justified, since SOT which drives the domain wall to move is proportional to J, and it contributes to the motion of domain wall given that the gradient of magnetic anisotropy does not exist. As to the track with magnetic anisotropy gradient, we found that when J is as small as $\pm 5 \times 10^{10}$ A/m^2, the gradient of the anisotropy constant has little effect on the motion of the domain wall. With the increase of J, it is clear that the gradient of the anisotropy constant affects the motion of the domain wall. Under negative J, the domain wall moves towards the direction of increasing anisotropy, and it moves slower with increasing a. In contrast, the domain wall moves faster towards the direction of decreasing anisotropy. In particular, unlike the uniform
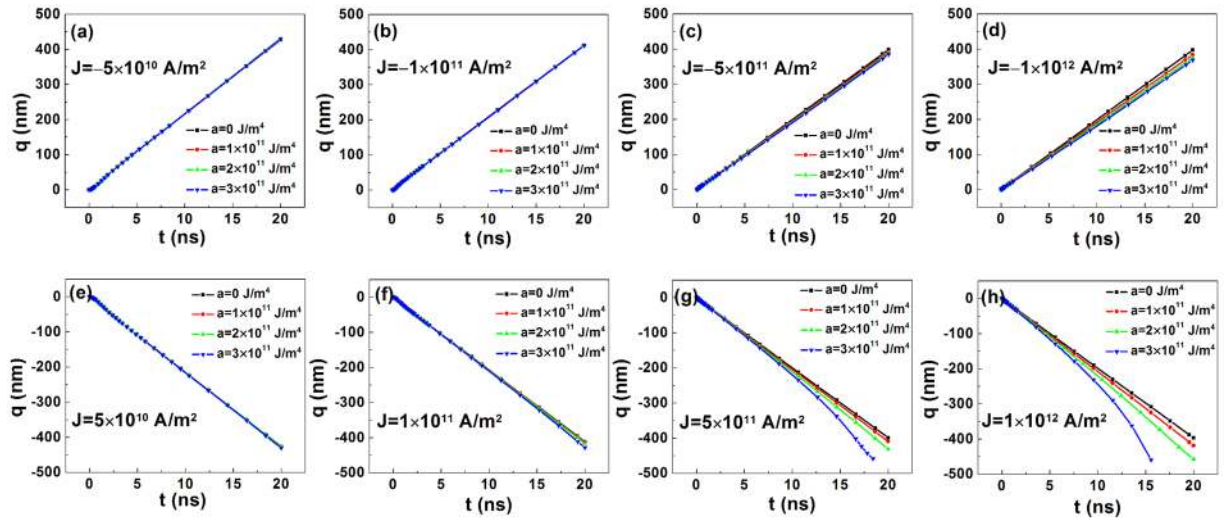
Figure 2. Change in time (t) of the central position of the domain wall (q) in the nanotracks with magnetic anisotropy gradient under current with different densities. The four figures in the first row show the $q−t$ curves under negative current with the current density (J) of (**a**) $−5 \times 10^{10}$ A/m², (**b**) $−1 \times 10^{11}$ A/m², (**c**) $−5 \times 10^{11}$ A/m², and (**d**) $−1 \times 10^{12}$ A/m² respectively. The four figures in the second row show the q-t curves under positive current with the J of (**e**) 5×10^{10} A/m², (**f**) 1×10^{11} A/m², (**g**) 5×10^{11} A/m², and (**h**) 1×10^{12} A/m² respectively. The slopes for the anisotropy constant (a) are 0 (marked in black), 1×10^{11} (marked in red), 2×10^{11} (marked in green), and 3×10^{11} J/m⁴ (marked in blue).
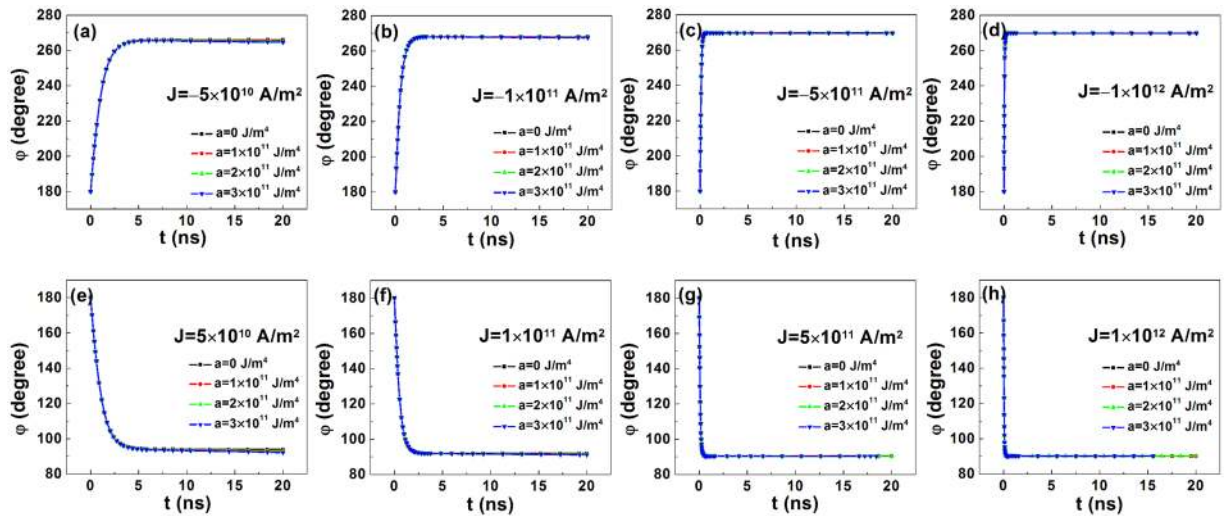

Figure 3. Time (t) dependence of the azimuthal angle (φ) of domain wall moments in nanotracks with magnetic anisotropy gradient under current with different densities. The four figures in the first row show that φ-t curves under negative current with respective current density (J) of (**a**) $−5 \times 10^{10}$ A/m², (**b**) $−1 \times 10^{11}$ A/m², (**c**) $−5 \times 10^{11}$ A/m², and (**d**) $−1 \times 10^{12}$ A/m². The four figures in the second row demonstrate that φ-t curves under positive current with respective J of (**e**) 5×10^{10} A/m², (**f**) 1×10^{11} A/m², (**g**) 5×10^{11} A/m², and (**h**) 1×10^{12} A/m². The slopes for the anisotropy constant (a) are 0 (marked in black), 1×10^{11} (marked in red), 2×10^{11} (marked in green), and 3×10^{11} J/m⁴ (marked in blue).

motion under negative J, the motion of the domain wall is accelerated under a strong positive J (1×10^{12} A/m²) when a is as large as 3×10^{11} J/m⁴.

The gradual changes of the azimuthal angle φ under different J are depicted in Fig. 3. When J takes a negative value, the moments in domain wall rotate to approximately 270°. By contrast, the moments rotate to approximately 90° under positive J. These figures are consistent with the reported results[9]. When J is as small as $\pm 5 \times 10^{10}$ A/m², the rotation is slower when compared with that under a stronger J, and φ is slightly smaller under a larger a. Under stronger current, the moments in the domain wall rotate very rapidly to their stable states, and the gradient of anisotropy has little effect on the final φ.
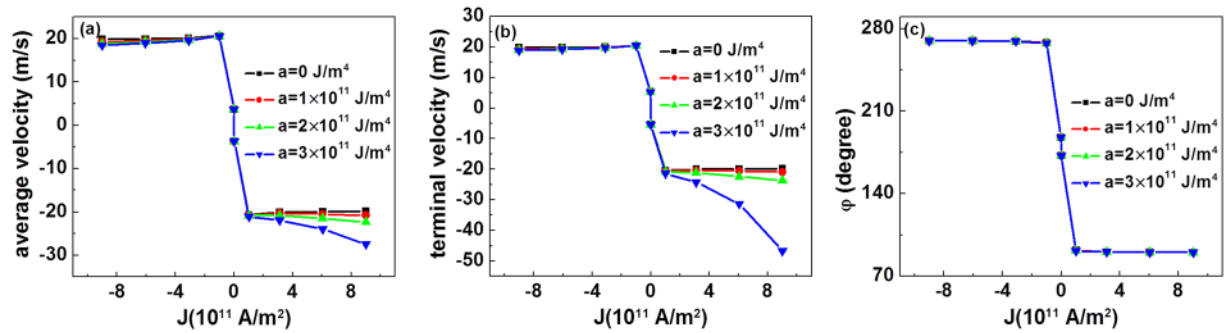
Figure 4. Current density dependence of the (**a**) average velocity, (**b**) terminal velocity, and (**c**) terminal azimuthal angle of domain wall moments in the nanotracks with magnetic anisotropy gradient.
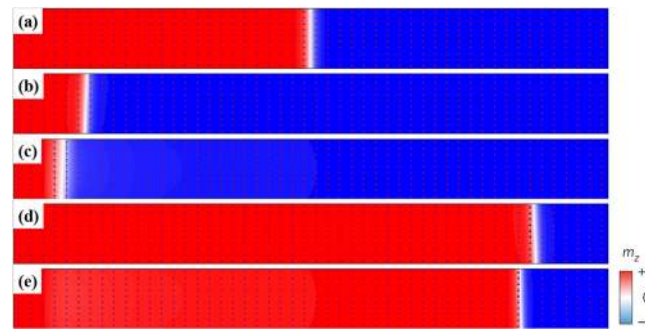

Figure 5. Micromagnetic configuration of SOT-induced domain wall motion in the 1000-nm-length track with piecewise anisotropy constant. (**a**) Snapshot of initial structure of a left-handed ($D < 0$) up-down domain wall. Snapshot of the domain wall moving after 20 ns under a current of $J = 5 \times 10^{11}$ A/m² in a track with (**b**) constant anisotropy ($a = 0$ J/m⁴) and (**c**) sloped anisotropy ($a = 3$ J/m⁴). Snapshot of the domain wall moving after 20 ns under a current of $J = -5 \times 10^{11}$ A/m² in a track with (**d**) constant anisotropy ($a = 0$ J/m⁴) and (**e**) sloped anisotropy ($a = 3$ J/m⁴).

We have also investigated the J-dependent velocity for the current-induced motion of the domain wall, including the average velocity during the entire 15-ns moving process and the terminal velocity at the final moving stage.

As observed in Fig. 4(a) and (b), when a is 0 J/m⁴, both the average velocity and the terminal velocity increase very rapidly to around ±20 m/s when J increases to $\pm 1 \times 10^{11}$ A/m². Such velocity is in accordance with the values reported for similar materials[9]. At higher current, however, both velocities exhibit a small decrease. A similar result of numerical calculation was reported[25, 26]. Under high current, the decrease of velocity is due to the transition of the domain-wall structure. At zero or very low current, the domain wall prefers a Néel-type structure due to the DMI, and the velocity of domain wall increases with the increase in J. At high current densities, to the contrary, under the action of very strong SOT, the domain-wall moments rotate towards the y axis, exhibiting a Bloch-type-like structure, as observed in Fig. 4(c). In this case, the velocity for the SOT-driven domain wall motion decreases[25, 26]. When a is non-zero, in the J range between 0 and $\pm 1 \times 10^{11}$ A/m², the gradient of the anisotropy constant has little effect on either velocity. However, the gradient of anisotropy clearly affects the velocity of the domain wall for larger J. At negative current, the domain wall moves towards high anisotropy, and the velocity decreases with increasing a. Under positive current, the domain wall moves towards the end with low anisotropy. In this direction, the reduction of anisotropy greatly affects the velocity. Under a current of $J = 1 \times 10^{12}$ A/m², when a increases from 0 to 3×10^{11} J/m⁴, the average velocity increases from approximately -20 m/s to approximately -30 m/s, and the terminal velocity is greatly enhanced from approximately -20 m/s to approximately -50 m/s. This increase in the terminal velocity is due to the non-linear q–t relationship shown in Fig. 2(h) under a large anisotropy slope. This result is important for applications because it indicates that the velocity of the domain wall can be more than doubled using anisotropy engineering, which is beneficial for enhancing the reading speed of domain-wall-type magnetic information storage media.

To justify the numerical calculation on the SOT-driven motion of the domain wall in a track with gradient of magnetic anisotropy, we have run related micro-magnetic simulation as reference. The results of micro-magnetic simulation on the piecewise constant function of K with $N = 17$, $\Delta x = 50$ nm, and $\Delta K = 0.15$ J/m³ in Eq. (19) are shown in Fig. 5. We selected an up-down domain wall structure as an example. In the initial state, the domain wall has a typical Néel-type structure with its moments pointing to the up side ($+z$) because of the negative D (Fig. 5(a)). Under positive current, the domain wall moves to the left side, and the φ of the moments in the domain wall is close to 90° (Fig. 5(b) and (c)). The reduction of the anisotropy constant clearly enhances the
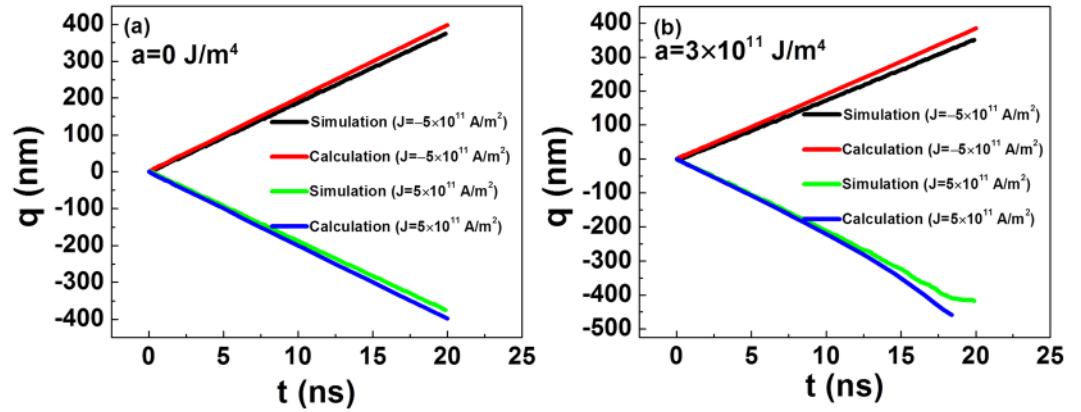
Figure 6. Comparison of numerical calculation and micro-magnetic simulation results for (**a**) $a = 0$ J/m⁴ and (**b**) $a = 3$ J/m⁴.

moving velocity and the width of the domain wall. In contrast, applying a positive current leads to the motion of domain wall towards the right side, where the higher anisotropy reduces the moving velocity of the domain wall, and the arrows in Fig. 5(d) and (e) indicate that φ is close to 270°. These results are consistent with those of the numerical calculations.

In Fig. 6, the simulation results are quantitatively compared with those of the numerical calculation. The micro-magnetic simulation and numerical calculation yield similar results. The difference between them is small and reasonable. This difference can be attributed to the following reasons: (1). Unlike the numerical calculation, in the simulation the changes of the anisotropy constant against x satisfies a piecewise constant function instead of a linear function. Therefore, the result approximation between the numerical calculation and the simulation for a small step size is well grounded. In addition to the step size of 50 nm shown in Figs 5 and 6, we also ran the simulation for the step sizes of 25 nm and 100 nm. The result (not shown) indicates that the difference of simulation results among different step sizes becomes negligible if the step size is 50 nm or smaller. Therefore, the step size of 50 nm is small enough for the simulation. Nevertheless, difference between the calculation and the simulation is still evident as shown in Fig. 6, and this difference is caused by the following factors. (2). In the numerical calculation, we do not consider the small tilting of the entire domain wall because of the weak DMI[9]. However, this small tilting can be observed in the simulation results (Fig. 5(b–e)). This tilting of domain wall may also reduce the velocity of domain wall motion as compared with that without the tilting, and this is consistent with the previous results[9, 13]. For a sample with higher DMI, such as Pt/CoFe, the tilting of the domain wall cannot be neglected because of the competition between the DMI and demagnetization energy of the domain wall[9, 13]. In this case, the tilting angle of the domain wall must be contemplated in numerical calculations to avoid errors. (3). In the simulation, the moments which are close to the boundaries are pinned by strong anisotropy, and this may act as a barrier to repel the domain wall when it is close to the end, resulting in the decrease of velocity.

Discussion

The current-driven motion of DW is dominated by the conjunctive action of several factors. For example, Li *et al.* discovered a screw-pitch effect (the combined motion of precession of DW moments and moving of DW center) as a result of the conjunct action of Gilbert damping and spin transfer torque (STT)[27]. In the SOT-induced DW motion, the DW is driven to move under the combined action of torque-like SOT (Equation 17), the gradient of anisotropy, and other contributions of free energy. To clarify the mechanism, we focus on the SOT and the gradient of magnetic anisotropy constants.

According to the Gilbert equation (Eq. 17), the effective field for SOT (H_{SO}) is written as:

$$\overrightarrow{H}_{SO} = \frac{\mu_B \theta_{SH} J}{\gamma_0 e M_S L_z} (\overrightarrow{m} \times \overrightarrow{\sigma}),$$ (20)

where μ_B, γ_0, M_S, L_z, and J are all positive (The variation of direction of current density changes the direction of σ); θ_{SH} and e are both negative. As to a negative θ_{SH}, when current is along $+x$ ($-x$) direction, σ is along $+y$ ($-y$) direction, and the angle (φ) of moment of DW is between 90° and 180° (180° and 270°) (Fig. 7(b) and (c) and Fig. 3). Therefore, when electrons move towards $-x$ ($+x$) direction, the H_{SO} is along $-z$ ($+z$) direction, pushing the DW to move in the $-x$ ($+x$) direction. In the track with constant magnetic anisotropy, the currents with the same strength and opposite signs offer the effective fields with identical strength and opposite directions, driving the domain wall to move in opposite directions at the same speed[3, 11, 23, 25, 28, 29].

When the magnetic anisotropy constant varies linearly with x, the change of domain wall energy against x can be phenomenologically converted into effective field (H_{eff}) expressed as[21]:

$$H_{eff} = \frac{1}{2M_S} \left(\frac{\partial \sigma}{\partial x} \right),$$ (21)
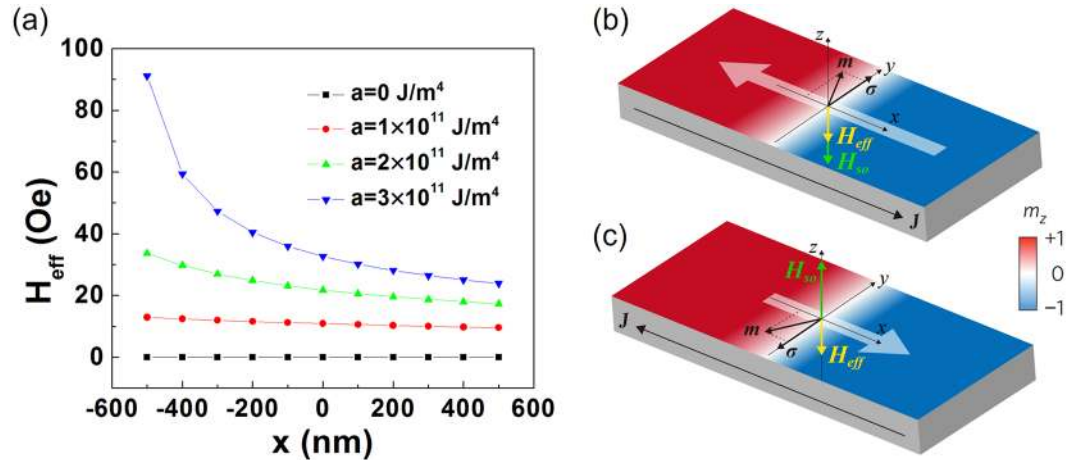
Figure 7. (**a**) The effective field due to the magnetic anisotropy gradient and its variation with x. The slopes for $K(x)$ function of (a) are 0 (marked in black), 1×10^{11} (marked in red), 2×10^{11} (marked in green), and 3×10^{11} J/m^4 (marked in blue). (**b**) and (**c**). Schematic of DW motion driven by both effective fields contributed from SOT (H_{SO}) and the gradient of magnetic anisotropy (H_{eff}). When current is along (**b**) $+$x direction, both H_{SO} and H_{eff} are in the $-z$ direction, while when current is along (**c**) $-$x direction, H_{SO} and H_{eff} have opposite directions.

where σ means the domain wall energy density, and its x-dependent term is $4\sqrt{AK_{eff}}$ $\left(K_{eff} = K - \frac{1}{2}\mu_0 M_S^2 = ax + b - \frac{1}{2}\mu_0 M_S^2 \right)$[21]. Therefore,

$$H_{eff} = \frac{a\sqrt{A}}{M_S\sqrt{ax + b - \frac{1}{2}\mu_0 M_S^2}}. \tag{22}$$

The variation of H_{eff} with x for different a is shown in Fig. 7(a). First of all, it can be observed that the constant magnetic anisotropy ($a = 0$ J/m^4) means zero H_{eff}. Moreover, H_{eff} goes up monotonously with the increase of a and the decrease of x. In particular, H_{eff} increases significantly with the decrease of x when the value of a reaches as large as 3×10^{11} J/m^4. This H_{eff} is along $-z$ direction so that the domain can move towards the track end with lower anisotropy ($-x$ direction)[21, 30].

At positive current, the domain wall moves towards negative x direction with weak magnetic anisotropy. In this case, both H_{eff} and H_{SO} share the same direction (Fig. 7(b)). As a result, the velocity of domain wall is larger than that for $a = 0$ J/m^4. As to a large gradient of magnetic anisotropy constant ($a = 3$ J/m^4), the H_{eff} is significantly enhanced with a decreasing x. Therefore, the domain wall moves at an ever increased rate. At negative current, the domain wall moves towards the positive x direction with stronger magnetic anisotropy energy under both H_{eff} and H_{SO}. The direction of H_{eff} is opposite to that of H_{SO} (Fig. 7(c)). Therefore, the velocity is comparatively reduced when compared to that for $a = 0$ J/m^4. Additionally, it is also observed that in regions with large positive x, H_{eff} can be approximately seen as a constant field, which ensures the uniform motion of the domain wall.

In a word, the symmetry of DW motion driven by H_{SO} is broken by the additional H_{eff} due to the gradient of magnetic anisotropy. It is interesting to see that similar magnetic field-induced symmetry breaking exists widely in nature, such as the magnetic field-induced asymmetric Josephson energy for a Josephson ratchet composed by a φ Josephson junction and a ferromagnetic barrier[31]. Additionally, besides the Thiele equations used in this paper, the current-driven motion of domain wall can also be investigated by some other methods. For example, Li *et al.* derived an effective Newton's equation for depicting the motion of a rigid-body DW driven by STT in a ferromagnetic nanowire with DMI[32]. The SOT-driven motion of DW in a track with the gradient of magnetic anisotropy using this method deserves further investigated.

Summary

In summary, using numerical calculations based on the collective coordinate model and micro-magnetic simulation, we investigated the SOT-induced motion of a domain wall in a nanotrack with weak DMI and magnetic anisotropy gradient. The domain wall exhibits a Néel-type structure due to the DMI, and the structure transforms into a Bloch-type-like one under SOT. The velocity of the domain wall motion is manipulated by the variation of the magnetic anisotropy constant along the track. The enhanced magnetic anisotropy constant acts as a barrier to hinder domain wall motion; however, reducing the magnetic anisotropy constants pushes the domain wall to move at a substantially higher speed. When the current density is 1×10^{12} A/m^2 and the slope for the space-variation of the anisotropy constant reaches 3×10^{11} J/m^4, the velocity can be more than doubled compared with that in the track with uniform anisotropy constant. The divergence between positive and negative J on the domain wall motion is attributed to the combined action of SOT and the x-dependent effective magnetic field which derives from the magnetic anisotropy gradient.

References

1. Parkin, S. S. P., Hayashi, M. & Thomas, L. Magnetic domain-wall racetrack memory. *Science* **320**, 190–194, doi:10.1126/science.1145799 (2008).
2. Haazen, P. P. *et al*. Domain wall depinning governed by the spin Hall effect. *Nat. Mater.* **12**, 299–303, doi:10.1038/nmat3553 (2013).
3. Ryu, K.-S., Thomas, L., Yang, S.-H. & Parkin, S. Chiral spin torque at magnetic domain walls. *Nat. Nanotechnol* **8**, 527–533, doi:10.1038/nnano.2013.102 (2013).
4. Emori, S., Bauer, U., Ahn, S.-M., Martinez, E. & Beach, G. S. D. Current-driven dynamics of chiral ferromagnetic domain walls. *Nat. Mater.* **12**, 611–616, doi:10.1038/nmat3675 (2013).
5. Franken, J. H., Herps, M., Swagten, H. J. & Koopmans, B. Tunable chiral spin texture in magnetic domain-walls. *Sci. Rep.* **4**, 5248, doi:10.1038/srep05248 (2014).
6. Yu, G. *et al*. Switching of perpendicular magnetization by spin-orbit torques in the absence of external magnetic fields. *Nat. Nanotechnol* **9**, 548–554, doi:10.1038/nnano.2014.94 (2014).
7. Thiaville, A., Rohart, S., Jué, É., Cros, V. & Fert, A. Dynamics of Dzyaloshinskii domain walls in ultrathin magnetic films. *EPL (Europhys. Lett.)* **100**, 57002, doi:10.1209/0295-5075/100/57002 (2012).
8. Emori, S. *et al*. Spin Hall torque magnetometry of Dzyaloshinskii domain walls. *Phys. Rev. B* **90**, 184427, doi:10.1103/PhysRevB.90.184427 (2014).
9. Martinez, E., Emori, S., Perez, N., Torres, L. & Beach, G. S. D. Current-driven dynamics of Dzyaloshinskii domain walls in the presence of in-plane fields: Full micromagnetic and one-dimensional analysis. *J. Appl. Phys.* **115**, 213909, doi:10.1063/1.4881778 (2014).
10. Torrejon, J. *et al*. Interface control of the magnetic chirality in CoFeB/MgO heterostructures with heavy-metal underlayers. *Nat. Commun.* **5**, 4655, doi:10.1038/ncomms5655 (2014).
11. Ryu, K.-S., Thomas, L., Yang, S.-H. & Parkin, S. S. P. Current Induced Tilting of Domain Walls in High Velocity Motion along Perpendicularly Magnetized Micron-Sized Co/Ni/Co Racetracks. *Appl. Phys. Express* **5**, 093006, doi:10.1143/APEX.5.093006 (2012).
12. Yu, J. *et al*. Spin orbit torques and Dzyaloshinskii-Moriya interaction in dual-interfaced Co-Ni multilayers. *Sci. Rep.* **6**, 32629, doi:10.1038/srep32629 (2016).
13. Boulle, O. *et al*. Domain wall tilting in the presence of the Dzyaloshinskii-Moriya interaction in out-of-plane magnetized magnetic nanotracks. *Phys. Rev. Lett.* **111**, 217203, doi:10.1103/PhysRevLett.111.217203 (2013).
14. Jué, E. *et al*. Domain wall dynamics in ultrathin Pt/Co/AlOx microstrips under large combined magnetic fields. *Phys. Rev. B* **93**, 014403, doi:10.1103/PhysRevB.93.014403 (2016).
15. Nasseri, S. A., Moretti, S., Martinez, E., Serpico, C. & Durin, G. Collective coordinate models of domain wall motion in perpendicularly magnetized systems under the spin hall effect and longitudinal fields. *J. Magn. Magn. Mater.* **426**, 195–201, doi:10.1016/j.jmmm.2016.11.081 (2017).
16. Zhang, Y. *et al*. Ring-shaped Racetrack memory based on spin orbit torque driven chiral domain wall motions. *Sci. Rep.* **6**, 35062, doi:10.1038/srep35062 (2016).
17. Schellekens, A. J., van den Brink, A., Franken, J. H., Swagten, H. J. & Koopmans, B. Electric-field control of domain wall motion in perpendicularly magnetized materials. *Nat. Commun.* **3**, 847, doi:10.1038/ncomms1848 (2012).
18. Lin, W. *et al*. Universal domain wall dynamics under electric field in Ta/CoFeB/MgO devices with perpendicular anisotropy. *Nat. Commun.* **7**, 13532, doi:10.1038/ncomms13532 (2016).
19. Ando, F. *et al*. Modulation of the magnetic domain size induced by an electric field. *Appl. Phys. Lett.* **109**, 022401, doi:10.1063/1.4955265 (2016).
20. Chiba, D. *et al*. Electric-field control of magnetic domain-wall velocity in ultrathin cobalt with perpendicular magnetization. *Nat. Commun.* **3**, 888, doi:10.1038/ncomms1888 (2012).
21. Yamada, K., Murayama, S. & Nakatani, Y. Magnetic domain wall motion in Co/Ni nanowires induced by a sloped electric field. *Appl. Phys. Lett.* **108**, 202405, doi:10.1063/1.4950865 (2016).
22. Nasseri, S. A., Sarma, B., Durin, G. & Serpico, C. Analytical Modelling of Magnetic DW Motion. *Phys. Procedia* **75**, 974–985, doi:10.1016/j.phpro.2015.12.133 (2015).
23. Martinez, E., Emori, S. & Beach, G. S. D. Current-driven domain wall motion along high perpendicular anisotropy multilayers: The role of the Rashba field, the spin Hall effect, and the Dzyaloshinskii-Moriya interaction. *Appl. Phys. Lett.* **103**, 072406–6, doi:10.1063/1.4818723 (2013).
24. Rohart, S. & Thiaville, A. Skyrmion confinement in ultrathin film nanostructures in the presence of Dzyaloshinskii-Moriya interaction. *Phys. Rev. B* **88**, 184422, doi:10.1103/PhysRevB.88.184422 (2013).
25. Rushforth, A. W. Domain wall motion driven by spin Hall effect—Tuning with in-plane magnetic anisotropy. *Appl. Phys. Lett.* **104**, 162408, doi:10.1063/1.4873583 (2014).
26. He, P.-B., Yan, H., Cai, M.-Q. & Li, Z.-D. Sustained chiral magnetic domain wall motion driven by spin-orbit torques under the tilted current. *EPL (Europhys. Lett.)* **114**, 67001, doi:10.1209/0295-5075/114/67001 (2016).
27. Li, Z.-D. *et al*. Screw-pitch effect and velocity oscillation of a domain wall in a ferromagnetic nanowire driven by spin-polarized current. *J. Phys.: Condens. Matter* **22**, 216001, doi:10.1088/0953-8984/22/21/216001 (2010).
28. Bang, D. *et al*. Enhancement of spin Hall effect induced torques for current-driven magnetic domain wall motion: Inner interface effect. *Phys. Rev. B* **93**, 174424, doi:10.1103/PhysRevB.93.174424 (2016).
29. Ryu, K. S., Yang, S. H., Thomas, L. & Parkin, S. S. Chiral spin torque arising from proximity-induced magnetization. *Nat. Commun.* **5**, 3910, doi:10.1038/ncomms4910 (2014).
30. Thiaville, A., Nakatani, Y., Miltat, J. & Suzuki, Y. Micromagnetic understanding of current-driven domain wall motion in patterned nanowires. *EPL (Europhys. Lett.)* **69**, 990–996, doi:10.1209/epl/i2004-10452-6 (2005).
31. Menditto, R. *et al*. Tunable φ Josephson junction ratchet. *Phys. Rev. E* **94**, 042202, doi:10.1103/PhysRevE.94.042202 (2016).
32. Li, Z.-D., Liu, F., Li, Q.-Y. & He, P. B. Dzyaloshinskii-Moriya domain wall resonance in ferromagnetic nanowires with a spin-transfer torque. *J. Appl. Phys.* **117**, 173906, doi:10.1063/1.4919676 (2015).

Acknowledgements

Author Contributions

Yue Zhang deduced the equations based on his idea and wrote the manuscript. Shi jiang Luo performed the micro-magnetic simulation and analyzed the simulation results. Xiaofei Yang supported the revision of the paper. Chang Yang solved the equations and revised the manuscript. All authors read and approve the final manuscript.

Additional Information

Competing Interests: The authors declare that they have no competing interests.

Publisher's note: Springer Nature remains neutral with regard to jurisdictional claims in published maps and institutional affiliations.